Marine Pollution Bulletin 213 (2025) 117602

Contents lists available at ScienceDirect

Marine Pollution Bulletin

journal homepage: www.elsevier.com/locate/marpolbul

Numerical modeling of the dispersion and accumulation of marine litter from the Dniester River in coastal areas of the northwestern Black Sea

Leidy M. Castro-Rosero [a,b,*], Ivan Hernandez [a], Marc Mestres [a], Maria Liste [a], Jose M. Alsina [a,c], Manuel Espino [a]

[a] Laboratori d'Enginyeria Marítima (LIM), Universitat Politècnica de Catalunya - BarcelonaTech (UPC), Departament d'Enginyeria Civil i Ambiental (DECA), C/ Jordi Girona 1-3, 08034, Barcelona, Spain
[b] Universitat de Barcelona (UB), Facultat de Ciències de la Terra, C/ Martí I Franqués, 08028, Barcelona, Spain
[c] Departament d'Enginyeria Gràfica i de Disseny (DEGD), Universitat Politècnica de Catalunya - BarcelonaTech (UPC), Avinguda Diagonal 647, 08034, Barcelona, Spain

ARTICLE INFO

Keywords:
Marine litter
Dniester River
Black Sea
Coastal numerical modeling
Sevastopol eddy
Suspended particulate matter
Satellite observations

ABSTRACT

This study investigates the transport and accumulation of Floating Marine Litter (FML) in the northwestern Black Sea, with a focus on the influence of the Dniester River and regional circulation patterns, including the Sevastopol Eddy. Two numerical modeling configurations (C1 and C2) are compared to assess their effectiveness in simulating FML dispersion. While both configurations show similar final beaching percentages, C2, which incorporates pre-calculated shoreline distances, can be more spatially accurate as it accounts for the complex shape of the coastline. The model's capability is validated through comparisons with previous models, satellite-derived Suspended Particulate Matter (SPM), and in situ observations from the 2017 EMBLAS campaign. These comparisons highlight FML accumulation patterns, particularly at the mouth of the Dniester River in the Zatoka region and in open waters within the Northwestern Shelf (NWS). The study suggests a correlation between satellite SPM observations and microplastic (MP) presence in coastal zones around the Dniester River, indicating avenues for future research. Understanding these dynamics is crucial for coastal management, with significant implications for environmental conservation strategies in the northwestern Black Sea.

1. Introduction

Marine litter poses a significant challenge to coastal ecosystems worldwide, impacting biodiversity, human health, and local economies. This issue is particularly acute in semi-enclosed seas like the Black Sea, where limited water exchange and high riverine input exacerbate litter accumulation. The Black Sea, one of the world's largest semi-enclosed seas, is profoundly influenced by its western and northwestern catchments, which account for over 80 % of its total basin (Karageorgis et al., 2009; Vespremeanu and Golumbeanu, 2018).

Among these catchments, the Danube, Dnieper, and Dniester rivers — considered some of the largest transboundary rivers in Europe — play a critical role in shaping the hydrodynamics and ecological characteristics of the northwestern Black Sea region. In addition to serving as vital sources of freshwater and particulate matter, these rivers act as conduits for pollutants from human activities, significantly contributing to the influx of litter into the sea. For instance, large rivers like the Danube and Dniester discharge an estimated 6 to 50 litter items per hour into the Black Sea (Lazăr, 2021; Lechner et al., 2014; Slobodnik et al., 2022; Strokal et al., 2022; Suaria et al., 2015).

Additionally, coastal areas, particularly those influenced primarily by rivers, receive the highest number of Floating Marine Litter (FML) and are thus the most vulnerable to its accumulation (Harris et al., 2021; Lebreton et al., 2019). Compared to other European seas, Black Sea beaches are the most littered, with a median value of 652 litter items/100 m (Slobodnik et al., 2022). Moreover, the coastal area of the northwestern Black Sea is heavily used for recreational activities, settlements, and agricultural land, thus further contributing significantly to coastal litter. According to Safranov et al. (2020), the annual volume of solid waste in the northwestern Black Sea region may reach 2.5 million tons, with plastic waste estimated to exceed 320 kton/y.

In particular, the coastline around the Dniester River and Odesa

* Corresponding author at: Laboratori d'Enginyeria Marítima (LIM), Universitat Politècnica de Catalunya - BarcelonaTech (UPC), C/ Jordi Girona 1-3, 08034, Barcelona, Spain.

E-mail address: lcastrro22@alumnes.ub.edu (L.M. Castro-Rosero).

https://doi.org/10.1016/j.marpolbul.2025.117602
Received 2 December 2024; Received in revised form 21 January 2025; Accepted 21 January 2025
Available online 5 February 2025
0025-326X/

(Ukraine) emerges as a focal point of study due to its complexity and surrounding pressures. This includes nearby protected areas of ecological and touristic importance, such as the Tuzlovski Lagoons National Park, which is home to significant biodiversity and serves as a vital habitat for numerous species (Shekk, 2015). On top of that, in the Odesa region, about 17 % of landfills fail to meet environmental hazard criteria, and inadequate waste management systems result in a high proportion of plastic in marine litter (Iemelianov et al., 2024; Safranov et al., 2020). This issue is exacerbated by the litter transported by the Dniester River, which originates in West Ukraine and Moldova, flowing southeastward before emptying into the Black Sea near Odesa (Lebedynets et al., 2005). The Dniester River flows through a highly urbanized region with expanding industries such as food production, wood processing, and mining. Additionally, the river faces pressures from agricultural runoff, urban wastewater discharges, and aquaculture (Lazăr, 2021).

Furthermore, the observations of Floating Marine Macro Litter (FMML) reported by González-Fernández et al. (2022) in the framework of the EMBLAS-II and EMBLAS-Plus projects (Slobodnik et al., 2022) reveal that high FMML densities were observed in the territorial sea (within 12 NM radius) near Odesa. The weighted average density of FMML was about 29 items/km^2, with peaks of up to 580 items/km^2 recorded in 2017 and 2019, where plastic items accounted for 96.6 %. In agreement, Cincinelli et al. (2021) reported that the highest abundance of microplastics (MP) in their study was found in sediments at the station near Odesa (25 m depth), with 390 items/kg, and at the station near the Dniester River (23 m depth), with 260 items/kg. These nearshore sediment samples showed ten times higher MP abundance compared to deep-sea sediment samples. In view of the above, the increasing accumulation of both floating and sedimentary ML in the aforementioned area is evident.

Numerical models have proven to be invaluable tools for understanding the transport of FML in the Black Sea. For instance, simulations conducted by Miladinova et al. (2020) show higher densities on the Northwestern Shelf (NWS), particularly during the summer season. Their climatological analysis indicates that the coastline around the Dniester River exhibits a high particle density. Additionally, simulations by Stanev and Ricker (2019) identified high-density areas around river mouths, with the northwest coast near the mouths of the Danube and Dniester being particularly notable for the highest concentration of beached particles.

More recently, previous regional simulations have also identified the northwestern Black Sea as a high-density area, especially due to the contribution of northern rivers (Castro-Rosero et al., 2023). In that study, a marine litter numerical model called LOCATE was used, which is specifically adapted for coastal regions and integrates Eulerian hydrodynamic data with Lagrangian simulations of virtual particles representing FML. Furthermore, Hernandez et al. (2024) have demonstrated the application of LOCATE at coastal scales by nesting hydrodynamic grids with varying resolutions, including a beaching module that calculated particle distance to the shore in real-time, thus providing detailed analyses of local processes near river mouths.

Assessing and validating the results of models in coastal areas is challenging without constant and continuous monitoring or available data. Therefore, the integration of satellite imagery data has emerged as a feasible and cost-effective method for detection and comparison with the models (Martínez-Vicente et al., 2019). Studies that use remote sensing data to map floating and beached ML have become more common in recent years (Veettil et al., 2022; Waqas et al., 2023).

Lastly, Atwood et al. (2019) found that remote sensing effectively captures river mouth discharge and MP accumulation patterns, aligning well with hydrodynamic models. They pointed out that although converting this to actual MP accumulation rates is still difficult, remote sensing provides finer spatial resolution and precise pictures of surface river plumes across wide areas. Piehl et al. (2020) were the first to establish a significant relationship between MP concentrations and water constituents in the Trave River in northern Germany. Their work laid the groundwork for satellite-based tracking of MP distribution using proxy indicators like Suspended Particulate Matter (SPM) or chlorophyll. Building on this, Sullivan et al. (2023) applied a similar approach in the Tamar estuary in the UK, using a satellite algorithm to estimate MP flux rates from the river. They confirmed a strong correlation between SPM and MP concentration, suggesting that remote sensing can serve as a proxy for MP in coastal locations. However, they emphasize that their results should not be applied without thorough evaluation, as each river system is unique.

The aim of this study is to use the LOCATE model with a coastal approach, using high-resolution nested grids for the area of the Dniester River mouth. We intend to evaluate the difference between the beaching conditions and compare our results with available SPM satellite observations and count data. With this approach, we expect to assess the behavior of our model in coastal areas with high-resolution data, contribute to a better understanding of the local processes in the northwestern Black Sea and validate our results using satellite data. In addition, this study aims to serve as input for decision-making processes that contribute to the better management of FML pollution in the northwestern Black Sea region. The paper is structured as follows: first, we present the methodology for nesting hydrodynamic data grids, followed by the simulation conditions in LOCATE and the satellite SPM imaging process. We then compare the simulation results with satellite and count data, analyze the results, and conclude with our final reflections.

2. Materials and methods

The present study uses the LOCATE v1.0 numerical model based on Parcels v2.4.2 detailed in Hernandez et al. (2024). This model was developed in the framework of the project “LOCATE: Prediction of Plastic Hot-spots in Coastal Regions using Satellite-Derived Plastic Detection, Cleaning Data, and Numerical Simulations in a Coupled System” and takes into account factors such as beaching and residence time (time that the particles remain in the water before they are beached on the shore) as well as allowing nesting of hydrodynamic grids of different resolutions and use of modeled current and wave data. This capability allows for a more accurate examination of physical processes at the coastal scale. The Black Sea regional adaptation of this model has been carried out in previous work by Castro-Rosero et al. (2023) mainly highlighting the importance of including Stokes drift in the simulation setup to avoid overestimating residence times.

In this exercise, LOCATE identifies beached particles by determining the position at which floating lagrangian elements transition from water to land based on a customizable beaching parameterization, removes them from the simulations, and records the beaching time and location of each one for further analysis. It’s important to note that this experiment does not consider beached particles re-suspension in the system and the particles used are virtual tracers without mass, size, shape, or buoyancy, simply following the surface flow. Because they lack mass and shape, processes like degradation, fragmentation, clustering, or sinking are not accounted for. Despite these limitations, using a Lagrangian model like LOCATE with virtual particles provides insights into general patterns and areas most affected by FML dispersion. Although this study does not investigate the properties or processes inherent in the litter, it provides valuable data on the behavior and distribution of FML in the northwestern Black Sea. Moreover, as they are virtual particles, their surface behaviors can be extrapolated to both macroplastics and microplastics (Alsina et al., 2020).

2.1. Nesting of hydrodynamic grids

Nesting grids have demonstrated better accuracy than coarse-resolution grids, particularly when evaluating dispersion by comparing drifter data with simulated trajectories (Hernandez et al.,

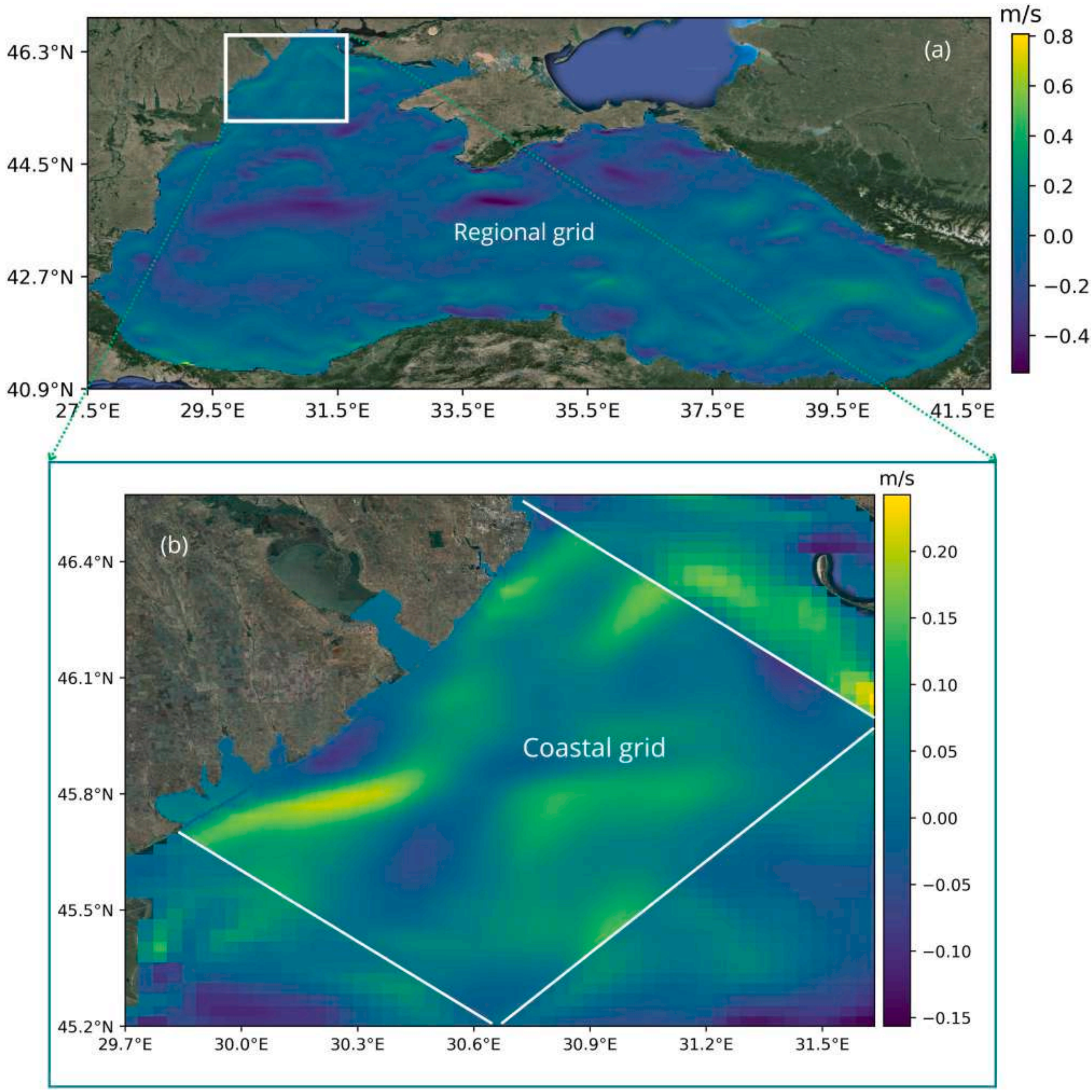

Fig. 1. Example of hydrodynamic grids for current velocity (m/s) on August 3rd 2017. Basemap sources: Esri, "World Imagery", DigitalGlobe, GeoEye, i-cubed, USDA FSA, USGS, AEX, Getmapping, Aerogrid, IGN, IGP, swisstopo, and the GIS User Community.

2024). Mesh nesting involved the utilization of regional current velocity and Stokes drift grids sourced from the Copernicus Marine Environment Monitoring Service (CMEMS) regular A-grids, with a horizontal resolution of 1/36° (2.5 km), and coastal-resolution C-grids from the COAWST model implemented by the Laboratori d'Enginyeria Maritima at the Universitat Politècnica de Catalunya (LIM/UPC) for the Dniester region, with a special resolution of 350 m. The regional grid covers the entire Black Sea, as shown in Fig. 1(a). An interpolation process transformed the C-grid mesh into an A-grid mesh (Delandmeter and van Sebille, 2019) using the psi points of the grid (nodes at the cell edges where spatial and temporal data are calculated). Additionally, a secondary interpolation filled gaps in the higher-resolution coastal scale grid with spatio-temporal data equivalent to that of the regional grid (Fig. 1(b)).

2.2. Lagrangian particle simulations

The simulation period extended from August 3rd to September 27th, 2017, coinciding with observational data collected in the northwestern Black Sea during the EMBLAS 2017 campaign, as documented by González-Fernández et al. (2022). Hourly particle releases originated from the grid cell closest to the mouth of the Dniester River (longitude 30.481°E, latitude 46.054°N) within the high-resolution grid. The number of particles released was determined from an estimated Dniester discharge of 0.25 kton/year (Strokal et al., 2022), following a similar methodology to previous works (Castro-Rosero et al., 2023). The rate of particle inflow varied daily based on the estimated flow of the Dniester River during those months.

A total of 15,059 particles were released during the 55-day simulation period, representing floating marine litter dispersion in the northwestern Black Sea. Two simulation types were conducted, each utilizing different beaching parameterization according to the methodology proposed by Hernandez et al. (2024). Configuration 1 (C1) considered a particle as beached when its x and y velocity components (u and v respectively) were approximately zero ($<=1 \times 10–16$ m/s) and the particle was located at a shoreline cell. Configuration 2 (C2) used the real-time particle distance to the shoreline in the simulation to assess when it crossed the land-water boundary using a pre-calculated distance grid. Coastline data were obtained from the Global Self-consistent, Hierarchical, High-Resolution Geography Database (GSHHG) and manually refined using open-source QGIS software.

2.3. Satellite data

The study included satellite data from the Sentinel-2 mission, comprising two identical satellites, Sentinel-2A and Sentinel-2B, managed by the European Space Agency (ESA) under the Copernicus Programme. These satellites offer systematic coverage of coastal waters up to 20 km from the shore, with a temporal resolution of 5 days at the equator and 2 to 3 days at mid-latitudes. Equipped with a Multispectral Instrument (MSI), each satellite captures sunlight reflected by the Earth, providing high spatial resolution (10 m, 20 m, or 60 m) for various spectral bands. The images used in the study were of MSIL1C type, indicating Level 1C processing, where data are ortho-rectified, ensuring geometric correction and referencing to a coordinate system. A total of 22 images were identified during the simulation period, of which 5 were discarded because visibility was obstructed by cloud cover, then processed in ESA's SNAP software using optical tools for water treatment and the C2RCC S2/MSI processor to obtain the Suspended Particulate Matter (SPM) concentration. The Case-2 Regional CoastColour (C2RCC) algorithm, detailed in Brockmann et al. (2016), is specifically designed for optically complex waters. While validation activities for this processor in the Black Sea are limited, studies such as Kyryliuk and Kratzer (2019) provide valuable insights into its performance in similar environments, such as the Baltic Sea, demonstrating its effectiveness in retrieving water quality parameters. The selected and discarded images are presented in the Table 1.

2.4. In situ data from ML observations

Observed marine litter data and their locations in the northwestern Black Sea used for comparison with our simulation results, were obtained from the work of González-Fernández et al. (2022) and through personal communication with the first author. The data were collected during the 2017 EMBLAS campaign using a methodology developed by the EU Joint Research Centre. This involved visual observations from vessels, trained observers, and using a mobile app to register and report Floating Marine Macro Litter (FMML) items. The observations applied a fixed-width strip transect methodology and recorded all macro litter items over 2.5 cm, occasionally using binoculars. Further details on the methodology can be found in González-Fernández et al. (2022).

Data from August and September 2017 were selected for analysis, covering 7 different days of observation, totaling approximately 16 h and 33 min, the observation periods ranged from about 19 min to about 3 h and 34 min.

For subsequent analysis of the obtained trajectories, comparisons were made using maps created with open-source QGIS software. The simulation domains, satellite images, and locations of the observations are shown in Fig. 2.

2.5. Identification of marine eddies from altimetry data

To assess whether the hydrodynamic model accurately replicates mesoscale phenomena, a qualitative comparison with altimetry data was performed. The altimetry data used in this study were obtained from the Copernicus Marine Environment Monitoring Service (CMEMS), specifically from the product "European Seas Gridded L4 Sea Surface Heights and Derived Variables," reprocessed from 1993 onwards with a resolution of 0.125°. The download domain is bounded by approximately 48.37°N to 39.98°N and 25.18° E to 43.15°E.

The identification of mesoscale eddies was performed using the Q parameter (Isern-Fontanet et al., 2003), defined as:

$$Q = -\left(\frac{\partial u}{\partial x}\right)^2 - \left(\frac{\partial v}{\partial x}\cdot\frac{\partial u}{\partial y}\right). \tag{1}$$

where u and v are the zonal and meridional geostrophic velocity components, respectively.

The use of this Q parameter (Isern-Fontanet et al., 2003) applies principles similar to the methodology introduced by Okubo (1970) and Weiss (1991) as a diagnostic tool to identify regions dominated by rotational motion. The Q methodology involves the following steps:

1. Convert latitude and longitude coordinates to a Cartesian grid.
2. Compute the spatial gradients of the geostrophic velocity components:

$$\frac{\partial u}{\partial x}, \quad \frac{\partial u}{\partial y}, \quad \frac{\partial v}{\partial x}, \quad \text{and} \quad \frac{\partial v}{\partial y}. \tag{2}$$

3. Calculate the Q parameter using these gradients.
4. Identify eddy structures by contouring the Q parameter. Eddies are typically identified where Q is positive, indicating that rotation dominates over deformation in the flow, which suggests the presence of coherent structures like eddies or vortices. This occurs when the shear terms $(dv/dx \cdot du/dy)$ are negative meaning that the rates of change of the velocity components in the x- and y-directions have opposite signs, and the rotation is stronger than the stretching of the flow. Conversely, when Q is negative, deformation dominates, and no coherent vortices are present.

3. Results and discussion

In this study, we conducted a qualitative comparison of spatial patterns observed in the simulated data with the features derived from satellite images and field observations.

Table 1
Summary of selected and discarded satellite images. Cloud cover percentage, satellite type, overpass time, and spatial resolution (10 m) are included for context.

Status	Satellite	Date of acquisition	Overpass time (UTC)	Cloud cover (%)	Spatial resolution (m)
Selected	Sentinel-2B	3/08/2017	08:45	0.89	10
Selected	Sentinel-2B	6/08/2017	09:00	0.09	10
Selected	Sentinel-2A	8/08/2017	08:46	0.19	10
Selected	Sentinel-2A	11/08/2017	08:56	0	10
Selected	Sentinel-2B	13/08/2017	08:50	0	10
Discarded	Sentinel-2B	16/08/2017	08:55	10.92	–
Selected	Sentinel-2A	18/08/2017	08:50	1.46	10
Selected	Sentinel-2A	21/08/2017	09:00	31.8	10
Selected	Sentinel-2B	23/08/2017	08:45	15.12	10
Selected	Sentinel-2B	26/08/2017	09:00	0	10
Selected	Sentinel-2A	28/08/2017	08:46	23.5	10
Selected	Sentinel-2A	31/08/2017	08:56	2.49	10
Selected	Sentinel-2B	2/09/2017	08:50	0.33	10
Discarded	Sentinel-2B	5/09/2017	08:55	46.35	–
Selected	Sentinel-2A	7/09/2017	08:50	1.08	10
Discarded	Sentinel-2A	10/09/2017	09:00	35.56	–
Discarded	Sentinel-2B	12/09/2017	08:45	80.36	–
Selected	Sentinel-2B	15/09/2017	09:00	0	10
Selected	Sentinel-2A	17/09/2017	08:46	0	10
Selected	Sentinel-2A	20/09/2017	08:56	21.96	10
Discarded	Sentinel-2B	22/09/2017	08:50	99.99	–
Selected	Sentinel-2B	25/09/2017	08:55	42.94	10

3.1. Comparative analysis of beaching configurations

At the end of the 55-day simulation, both configurations (C1 and C2) showed highly similar outcomes regarding residence time (the duration before beaching occurs), distance traveled (trajectory length), and percentage of beaching. Table 2 presents the maximum, minimum, and mean values of these outcomes. The standard error of the mean values (SEM) defined as:

$$SEM = \frac{\sigma}{\sqrt{n}}, \tag{3}$$

where σ represents the standard deviation of the sample and n is the sample size. In these results, SEM value indicates moderate precision for both simulations. A slightly lower SEM was observed for simulation C2.

The remaining floating particles were distributed in the northwest area, moving to the southwest. The simulation period seems insufficient for these particles to strand on distant shores, therefore all particles remain in the vicinity of the Dniester River, within the coastal areas of the Bilhorod-Dnistrovskyi district (Fig. 3(a) and 3(b)).

The highest concentrations of particles were found in the areas surrounding the river mouth, mostly towards the south. The coastal region of Zatoka exhibited the highest density of beached particles per km^2, with values reaching up to 1870.29 particles/km^2 in configuration C2 and a maximum of 1504.7 particles/km^2 in configuration C1. This discrepancy represents one of the main differences observed between the results of the configurations.The particle concentration gradually decreases along the coast towards the Tuzla group of lagoons (which includes the Burnas, Alibey, and Shagany lagoons), passing by the Budaki lagoon (Fig. 3(c) and 3(d)).

Residence times were comparable between configurations, with C1 slightly longer by 1.63 h, averaging 1 day and 5 h (Table 2). Figs. 3(e) and 3(f) illustrate residence times, showing that the first 7 km of the coast (from Zatoka to the edge of the Budaki lagoon) are covered in approximately 2 days while reaching the coast at the edge of the Burnas lagoon takes between 6 and 8 days. The distance traveled exhibits a similar pattern, with particles arriving in the Zatoka region having traveled <100 km, and those reaching the Burnas lagoon traveling between 200 and 300 km before beaching (Fig. 3(g) and 3(h)).

Another difference between the configurations is the spatial distribution: C1 shows particles in the Budaki lagoon and other sectors, utilizing velocity data from the hydrodynamic grid across its domain. In contrast, C2 models beached particles to remain at the beach border, defined by the 80–200 m wide barrier separating the lagoon, resulting in a more realistic outcome. Thus, while the overall difference in beaching quantification is not significant, the C2 configuration is more accurate in determining final locations on coastal scales because it takes the shape of the coastline into account.

Six particles were identified for their longest traveled distance before reaching the coast (Fig. 4(a)). These particles were released on September 12th between 12:00 h and 18:00 h and took about 14 days to reach the coast. These results are also similar for both simulations and their trajectories show that they were trapped in a vortex between the 18th and 23rd, and then were driven towards the coast beaching on the 26th. A comparison with altimetry data using the Q parameter (Fig. 4(b)) confirmed the presence of a vortex (red) in this area, which was accurately represented in the current field used in the modeling (black vectors), explaining this behavior.

3.2. Dniester River plume trajectory vs simulation C2 results

The release of particles from the river was compared with images showing the plume of Suspended Particulate Matter (SPM) derived from multispectral Sentinel observations. Considering the hourly output of particles, those between 08:00 h and 10:00 h UTC were selected to coincide with the satellite's passage between 8:45 h and after 9:00 h UTC. Note that UTC differs from local time by +2 h. Figs. 5 and 6 displays eight out of the 17 images for configuration C2, the remaining nine images are available in Appendix A.11.

These images reveal consistency between the simulated particles (shown in green) and the Dniester River plume (depicted in orange (depicted in orange, representing SPM concentrations ranging from 2.25 g/m^3 to over 5.77 g/m^3), particularly in terms of the extent of particle dispersion. They illustrate how particles tend to remain close to the source, resulting in the highest concentrations near the river mouth in most instances.

In the image for August 3rd (Fig. 5(a)), an expansion of the plume towards the northern area is observed. This SPM concentration could potentially be residual from previous days outside the simulation period. Additionally, a high concentration of SPM is observed in the area between 30.7°E and 31°E longitude and latitudes of 46.1°N and higher, which is presumed to originate from another source like the Dnieper-Bug estuary located in northern Ukraine, another major contributor to the northwestern Black Sea.

Furthermore, the alignment with the plume's direction is clearly observed in Fig. 5(b), 6(a), and 6(c), especially in the latter, where the southward vortex observed during that period is accurately simulated.

Regarding the patterns of arrival at the coast, it is important to note

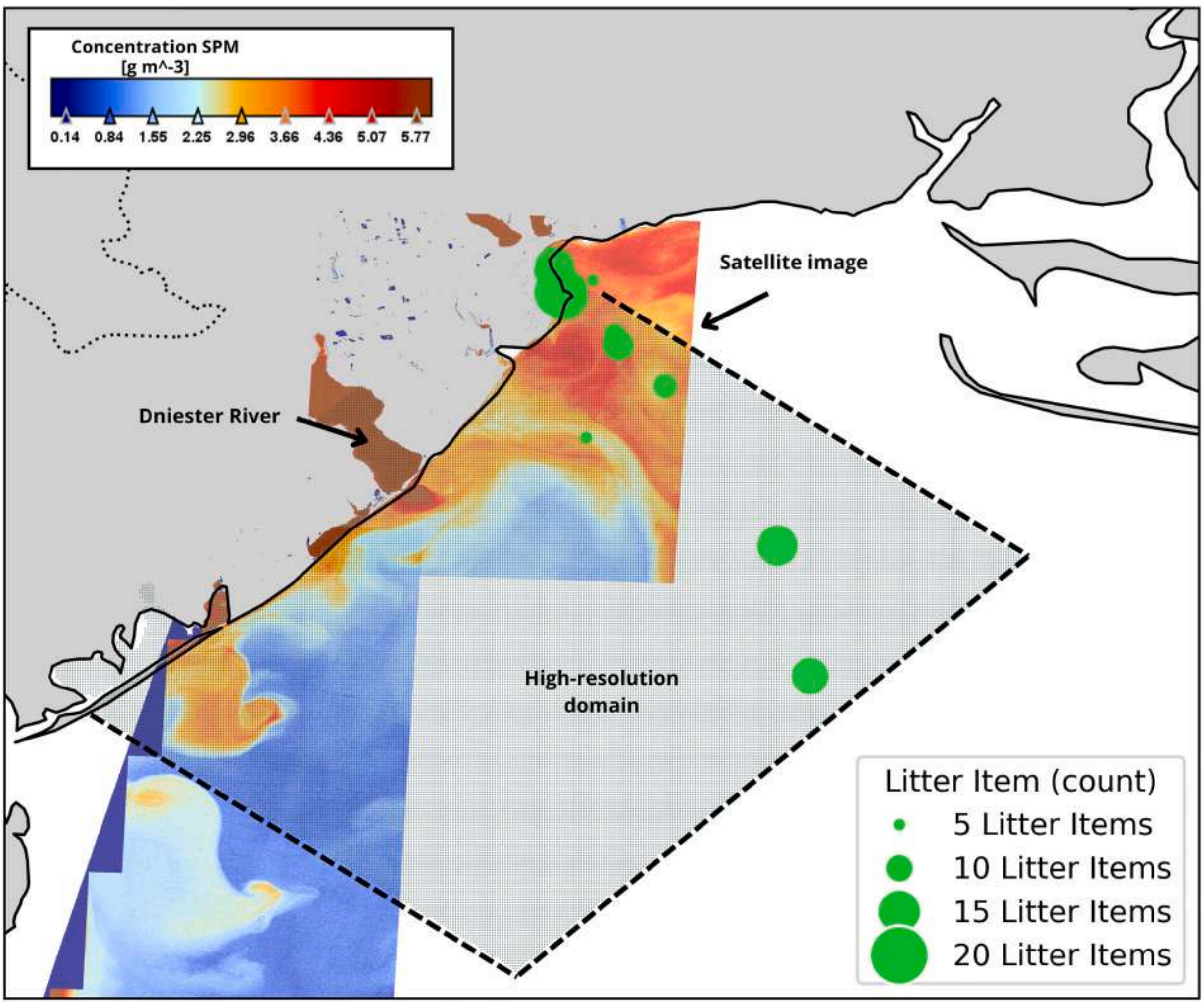

Fig. 2. Counts of Floating Marine Macro Litter (FMML) during EMBLAS campaign (August and September 2017), hydrodynamic data domain and satellite-derived information of Suspended Particulate Matter (SPM) in g/m^3.

Table 2
Results of the analysis of the percentage of beached particles, residence time in hours (minimum, maximum, and mean), distance traveled in kilometers (minimum, maximum, and mean), and standard error of the mean (SEM) for both simulation configurations (C1 and C2).

Type of simulation	Beaching amount (%)	Minimum residence time (h)	Maximum residence time (h)	Mean residence time (h)	SEM residence time	Minimum distance (km)	Maximum distance (km)	Mean distance (km)	SEM distance
C1	77.62	1	344.25	31.03	0.33	2.36	467.46	38.46	0.42
C2	77.36	1	342	29.4	0.32	2.19	465.07	36.6	0.41

that the simulation is configured to record the locations and arrival times of particles that beach and subsequently remove them from the simulation to expedite calculations. Therefore, to compare with the SPM concentrations observed on the coast, it is necessary to include simulated particles from previous days that could have arrived there. Figs. 7 (a) and 7(b) depict comparisons that include particles from August 10th for Fig. 7(a) and from August 29th for Fig. 7(b). This approach demonstrates that the accumulation patterns of simulated particles on the coast correspond to the direction and high concentrations of SPM plumes observed in satellite images. Overall, the qualitative evaluation provides valuable insights into how effectively the simulation captures the dynamics of particle dispersion compared to observed SPM plumes.

3.3. Comparison of simulated particle trajectories with observed plume dynamics in the northwestern area

At a larger scale, a comparison was made using available satellite images covering a wider area of the northwestern zone to evaluate the agreement between the trajectory of the observed plume and the simulated particles. Satellite images were obtained for August 28th (Fig. 8(a)), September 7th (Fig. 8(b)), and September 17th (Fig. 8(c)). These images illustrate the formation of vortices that progressively expand over time. One vortex, in particular, is highlighted (marked with red boxes) and shows good agreement with the simulated particle positions on the corresponding dates (Fig. 8(d), 8(e), and 8(f)). The particles also appear to expand as the vortex evolves over time.

The presence and dynamics of these vortices were further validated by comparing them with Q parameter values derived from daily altimetry data. This validation is visually represented by overlaying Q parameter contours onto the mean daily velocity field used in our simulations (Fig. 8(g), 8(h), and 8(i)).

For August 28th, the vortex center observed in Fig. 8(a) is approximately located at 45.7°N latitude and 31.0°E longitude. Simulated particles are shown to cluster near this center (Fig. 8(d)), and a nearby zone of positive Q is also evident in Fig. 8(g). It is worth noting that the daily temporal resolution of the altimetry data may limit precision when comparing with specific hourly simulation outputs. On September 7th, a vortex center located near 45.6°N latitude and 31.3°E longitude is well-replicated in the simulation, with particles expanding around this center (Fig. 8(e)). This vortex is also reflected as a nearby positive Q zone in Fig. 8(h). By September 17th, the vortex has expanded, with its center located at approximately 45.7°N latitude and 31.4°E longitude. Simulated particles are shown aggregated and distributed around this center (Fig. 8(f)), which corresponds to an extensive positive Q zone in Fig. 8(i).

Areas of vorticity (indicated by positive Q) serve as a potential proxy for mapping particle distribution when the SPM signal diminishes. For instance, particle aggregation observed in Fig. 8(d) at coordinates 30.7°E longitude and 45.3°N latitude aligns well with a vorticity zone indicated by the Q parameter in Fig. 8(g).

This vortex activity is associated with one of the most notable eddies in the Black Sea: the stationary Sevastopol anticyclone. Summer conditions—warm temperatures, a strong Rim Current, and significant mesoscale eddy activity—favor its formation and maintenance (Oguz et al., 1994; Kubryakov and Stanichny, 2015; Sadighrad et al., 2021; Ginzburg et al., 2002; Zhou et al., 2014). According to a recent detailed analysis by Kubryakov et al. (2024), the Sevastopol eddy stabilizes near the continental slope in early summer, constrained from moving westward by topography. This interaction generates submesoscale cyclonic eddies (SCEs), crucial for the Sevastopol eddy's dynamics. By late summer and early autumn (August–September), these SCEs intensify and merge into a vortex dipole with the Sevastopol eddy, drifting southwest due to internal forces. As a result, the separation process spans months, involving the development of attached SCEs, which dissipate energy and diminish the eddy's intensity further west.

On the other hand, findings from previous regional modeling studies highlight the significant influence of vortex activity in the northwest zone on the accumulation of Floating Marine Litter (FML) in this region. Miladinova et al. (2020) discusses the prevalence of anticyclones near the Danube and Dniester regions, leading to the formation of FML clusters in summer. These clusters are attributed to the Sevastopol anticyclonic eddy, which transports particles from the eastern part of the NWS and shelf break to the western region of the Rim Current.

Additionally, previous regional modeling work using LOCATE (Castro-Rosero et al., 2023) showed that, although a homogeneous particle distribution typically leads to the highest accumulation in the southwestern region following the cyclonic circulation of the Rim Current, the introduction of particles released from rivers changes this regional accumulation pattern. After a year of simulation, the northwestern region ends up with the highest percentage of particles. This is likely due to two factors: the high volume of particles from rivers in this area, including those with the most significant FML transport, and the tendency for more particles to become trapped in the vorticity phenomena or eddies generated by anticyclonic activity in this zone. For instance, in the case of the Dniester River, this leads to a rapid transport of particles to the coast. Moreover, Stanev and Ricker (2019) shows low dispersion of simulated particles originating from the Dniester River, noting that particles are more likely to beach to the right of the river mouth when viewed from the sea, consistent with the cyclonic circulation pattern. These observations align well with our results.

Furthermore, results of LOCATE regional simulations revealed that simulated particles from the Dniester River had the shortest arrival time for the first particle, at 5 h, and a maximum residence time of 184 days over a one-year simulation period, the lowest among the rivers studied (Castro-Rosero et al., 2023). In the present study using high-resolution data grids, the arrival time of the first particle was reduced to 1 h, likely due to the inclusion of more complex meso- and submesoscale dynamics not represented in the previous regional resolution.

These findings further support that the activity of the Sevastopol anticyclonic eddies not only impacts cross-shelf exchanges and nutrient fluxes but also significantly influences the movement of FML. Furthermore, the alignment of the simulated particles with observed SPM plumes, specific positive Q parameter zones derived from altimetry, and consistency with previous findings underscores the model's ability to capture and reproduce the general patterns of complex hydrodynamic behavior in the northwest zone. Although the Q parameter does not consistently correlate with all particle aggregations, it serves as an additional proxy for identifying vorticity zones that influence the coastal dynamics of FML dispersion.

3.4. Dispersion patterns and accumulation zones of FML

As mentioned earlier, the particles that remained floating in the

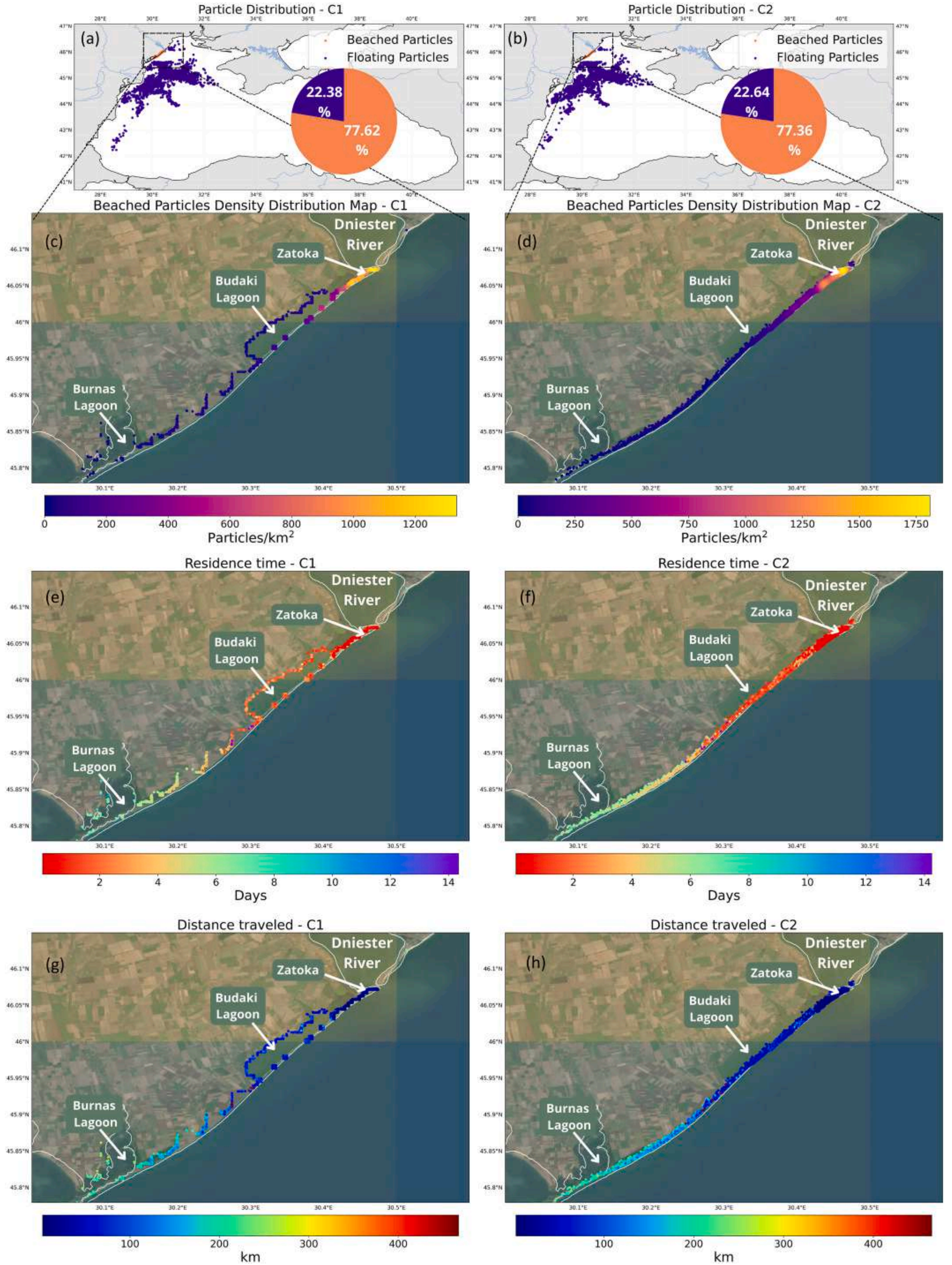

(caption on next page)

Fig. 3. Distribution of beached and floating particles at the end of the simulation for configuration C1 (a) and C2 (b). Panels (c) and (d) display the particle density (particles/km^2) on the coast for each configuration. Panels (e) and (f) illustrate the residence time of particles (days) upon reaching the coast for each configuration. Panels (g) and (h) present the distance traveled (km) by the particles upon reaching the coast for each configuration. Basemap sources: Esri, "World Imagery", DigitalGlobe, GeoEye, i-cubed, USDA FSA, USGS, AEX, Getmapping, Aerogrid, IGN, IGP, swisstopo, and the GIS User Community.

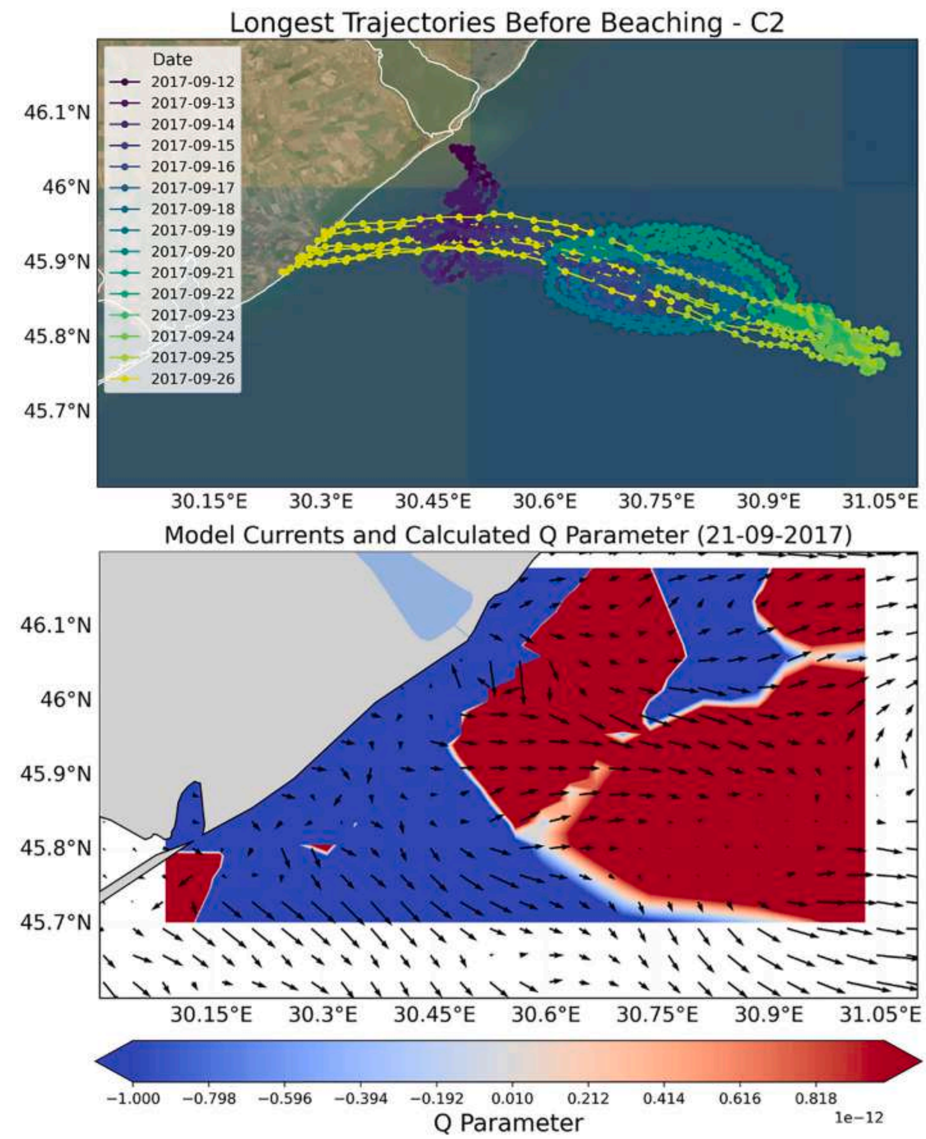

Fig. 4. (a) Trajectories of the particles that traveled the longest distance before beaching on the coast. The colors of the trajectories represent the time elapsed, with the legend indicating the corresponding colors for each day. (b) Currents field used in the model and the Q parameter. The colour map represents the values of the Q parameter, where red indicates positive values and the presence of vortices. The vectors in black indicate velocity components. Basemap sources: Esri, "World Imagery", DigitalGlobe, GeoEye, i-cubed, USDA FSA, USGS, AEX, Getmapping, Aerogrid, IGN, IGP, swisstopo, and the GIS User Community. (For interpretation of the references to colour in this figure legend, the reader is referred to the web version of this article.)

simulation predominantly stayed in the northwestern area, following the anticyclonic activity of the Sevastopol Eddy, and a few particles continued southward, following the cyclonic activity of the Rim Current. Among these floating particles, it is observed that as the simulation progresses beyond August 22nd, additional areas of high-density accumulation began to form not only near the mouth but also in the open water to the northwest, as evidenced in Fig. 9.

The effects of vorticity centers dynamics can lead to either beaching or dispersion of particles, depending on their position relative to the vortex, along with the influence of Stokes drift, which has been suggested in previous studies to contribute to particle beaching (Castro-Rosero et al., 2023). Particles on the outer edges of the vortex are more likely to be transported towards the coast and undergo beaching, while those closer to the vortex center tend to remain trapped and dispersed (D'Asaro et al., 2018). Strong, long-lasting vortices enhance dispersion by trapping particles, whereas weaker vortices, combined with Stokes drift, allow particles to be carried to shore by dominant coastal currents. This interplay results in vortices facilitating both dispersion and beaching based on these factors.

These findings align with observations from the study by González-Fernández et al. (2022) during the 2017 EMBLAS campaign. Higher concentrations of Floating Marine Macro Litter (FMML) were calculated for September 6th at the points with coordinates 45.96°N, 31.19E° and 45.71°N, 31.25°E during their observation transect. These higher

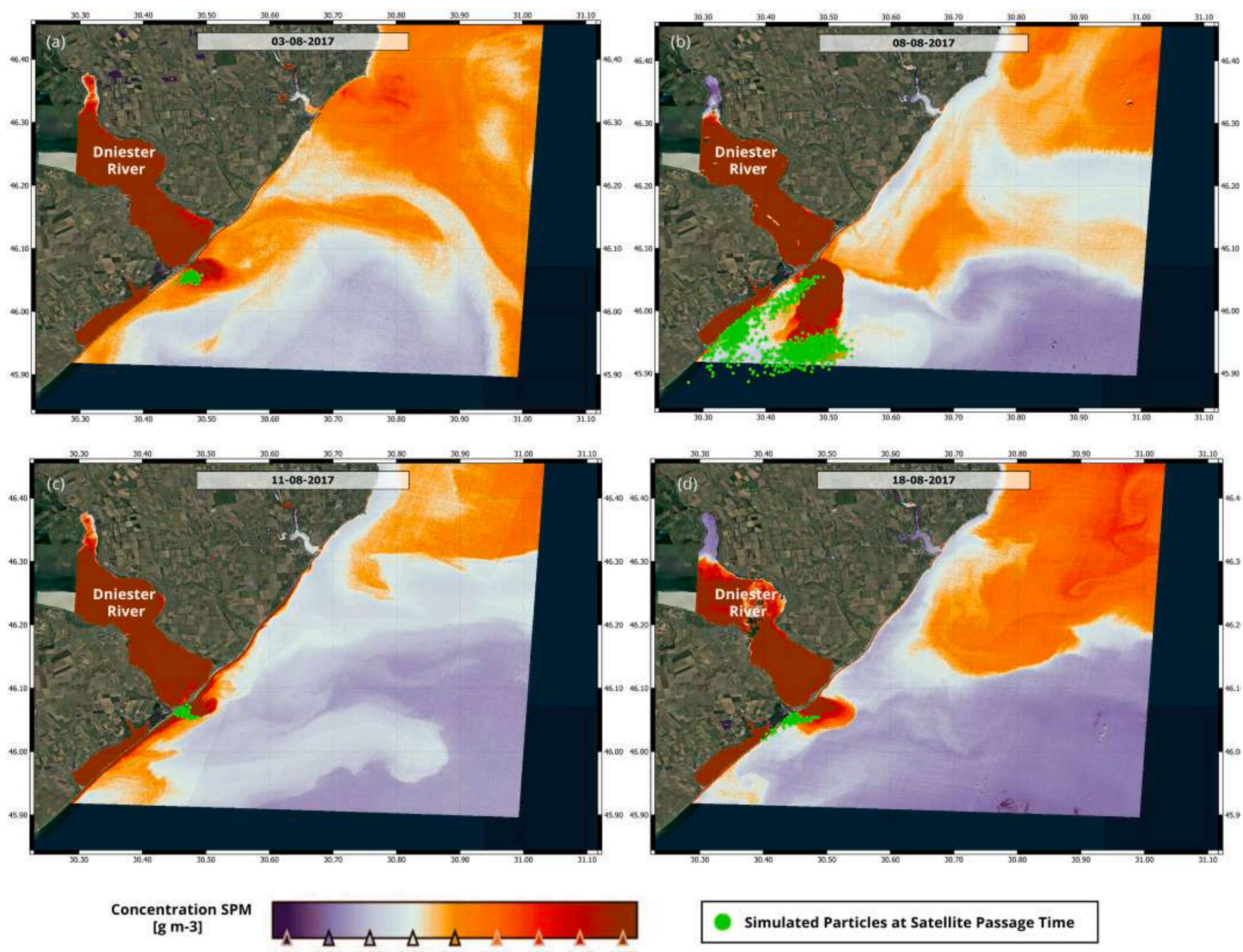

Fig. 5. Comparison between the results of the C2 (green particles) simulation and the SPM (Suspended Particulate Matter) plume from the mouth of the Dniester River, extracted from Sentinel-2 satellite imagery. Dates from August 3rd to August 18th. Basemap sources: Esri, "World Imagery", DigitalGlobe, GeoEye, i-cubed, USDA FSA, USGS, AEX, Getmapping, Aerogrid, IGN, IGP, swisstopo, and the GIS User Community. (For interpretation of the references to colour in this figure legend, the reader is referred to the web version of this article.)

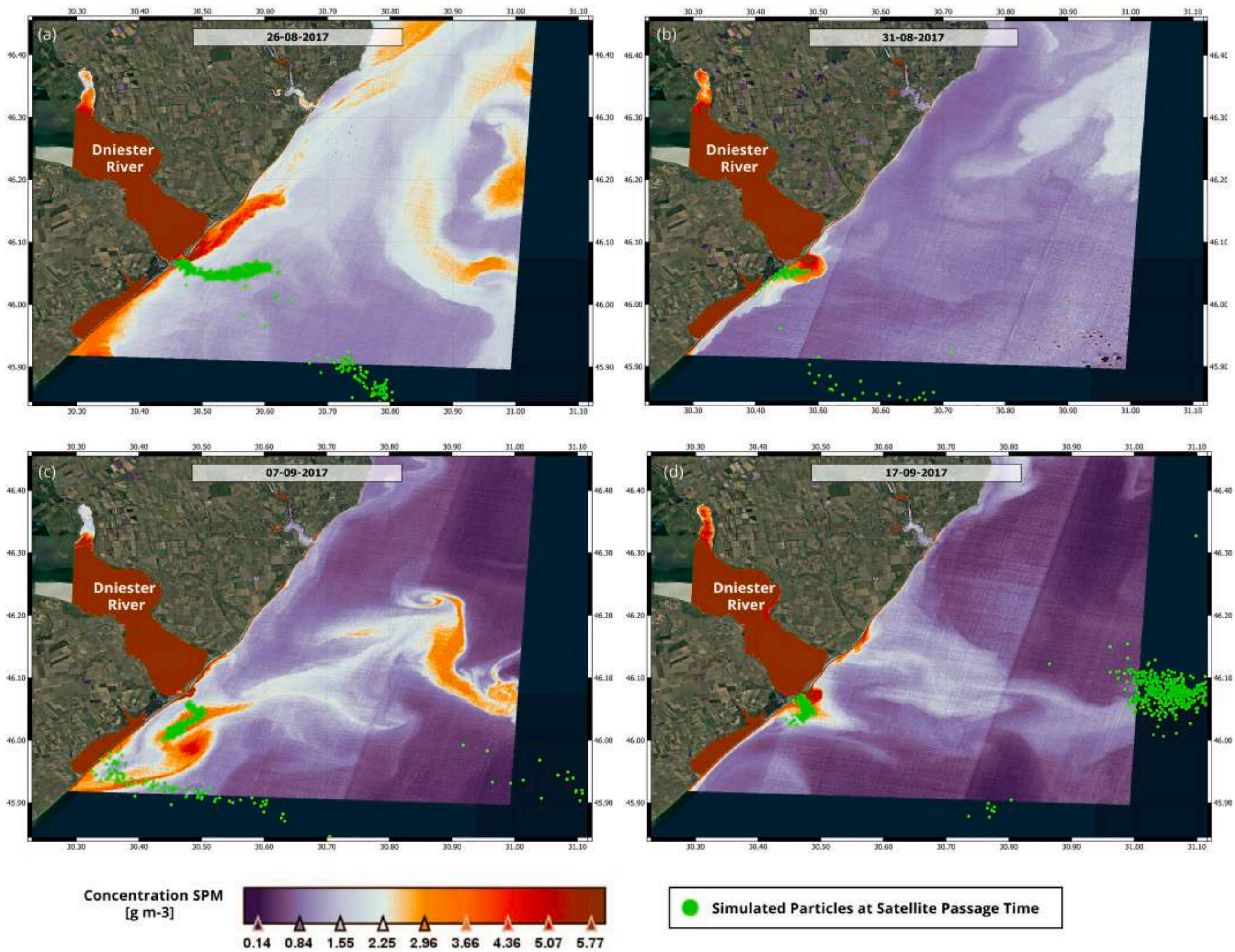

Fig. 6. Comparison between the results of the C2 (green particles) simulation and the SPM (Suspended Particulate Matter) plume from the mouth of the Dniester River, extracted from Sentinel-2 satellite imagery. Dates from August 26th to September 19th. Basemap sources: Esri, "World Imagery", DigitalGlobe, GeoEye, i-cubed, USDA FSA, USGS, AEX, Getmapping, Aerogrid, IGN, IGP, swisstopo, and the GIS User Community. (For interpretation of the references to colour in this figure legend, the reader is referred to the web version of this article.)

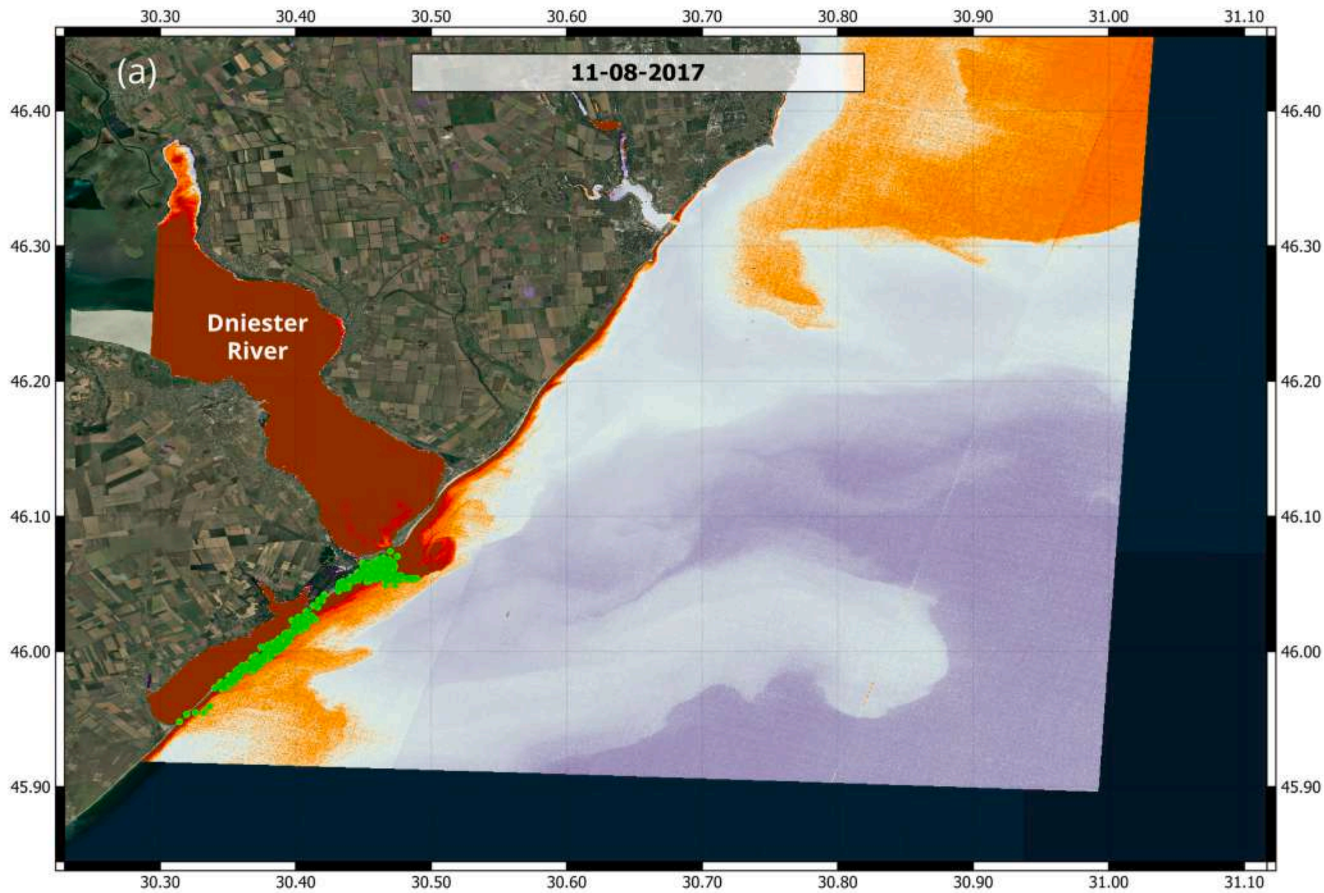

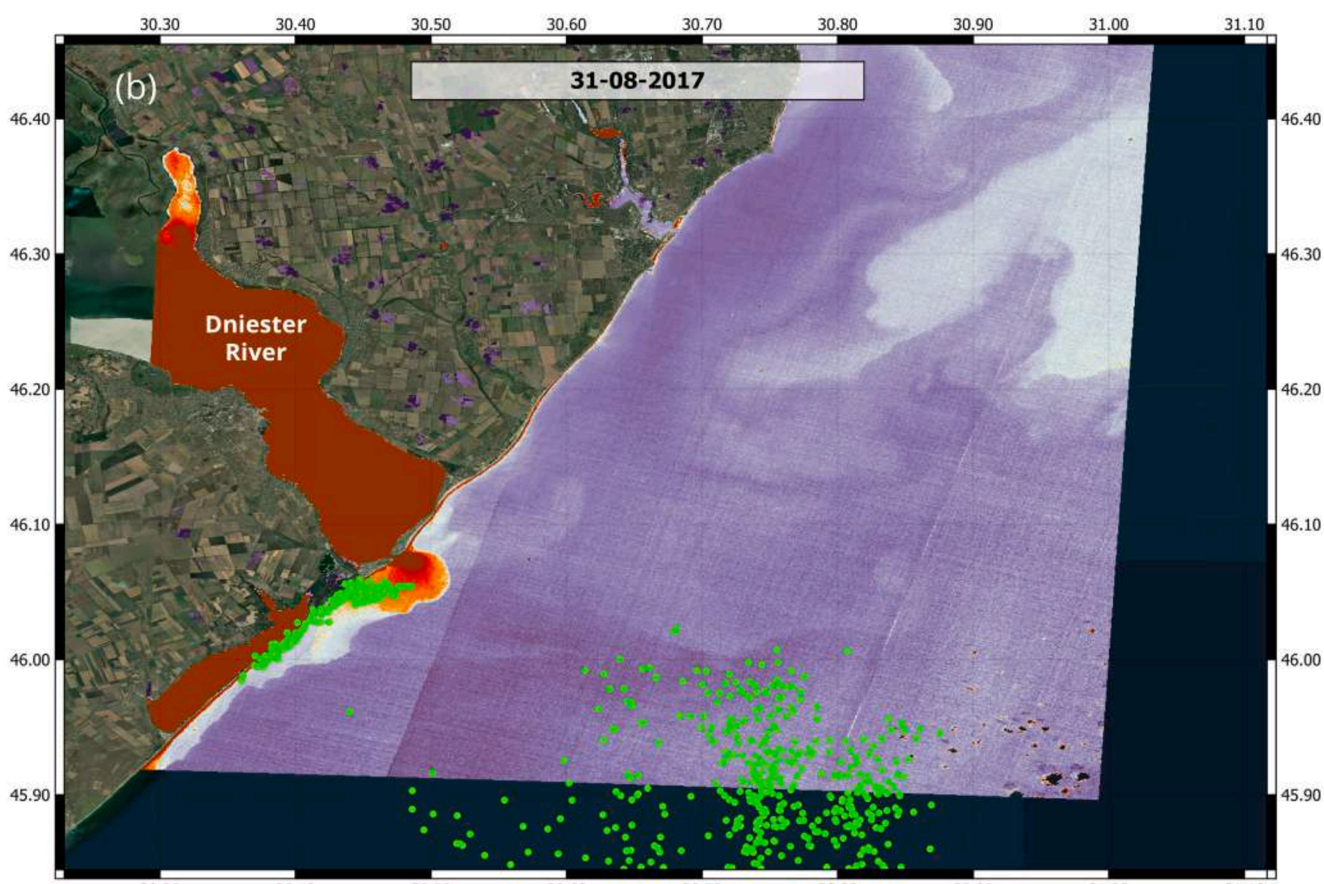

(caption on next page)

Fig. 7. Comparison between the simulation results C2 (green particles) and SPM (Suspended Particulate Matter) on the coast for August 11th taking into account beached particles since August 10th and for August 31st taking into account beached particles since August 29th. Basemap sources: Esri, "World Imagery", DigitalGlobe, GeoEye, i-cubed, USDA FSA, USGS, AEX, Getmapping, Aerogrid, IGN, IGP, swisstopo, and the GIS User Community. (For interpretation of the references to colour in this figure legend, the reader is referred to the web version of this article.)

concentrations were noted near vorticity zones, coinciding with the area where an SPM image obtained a day before the observations (Fig. 10(a)) shows the formation of a vorticity center. Similarly, our density analysis of particles on the same counting day reveals high-concentration areas near the observation points (Fig. 10(b)).

While our model captures the general trends of observed transport and accumulation patterns, it relies on the assumption that microplastics and macroplastics exhibit similar transport behaviors to the simulated Lagrangian particles, which represent neutrally buoyant floating debris. Although this assumption simplifies the modeling process, it is important to evaluate its implications for interpreting the results.

Microplastics and macroplastics differ significantly in size, shape, density, and their response to environmental forces. For example, macroplastics are more influenced by windage due to their larger surface area, as noted by Forsberg et al. (2020). While our model incorporates Stokes drift to approximate wind-driven motion, it does not explicitly differentiate between the transport behaviors of microplastics and macroplastics.

Buoyancy also plays a critical role in the vertical and horizontal distribution of particles. Macroplastics typically remain at or near the surface, whereas microplastics are subject to vertical mixing driven by biofouling, agglomeration with organic matter, or sediment interactions (van Sebille et al., 2020). By treating all particles as floating on the surface, our simulations may overestimate the dispersion of microplastics in open waters while underestimating their potential for settling or submerging.

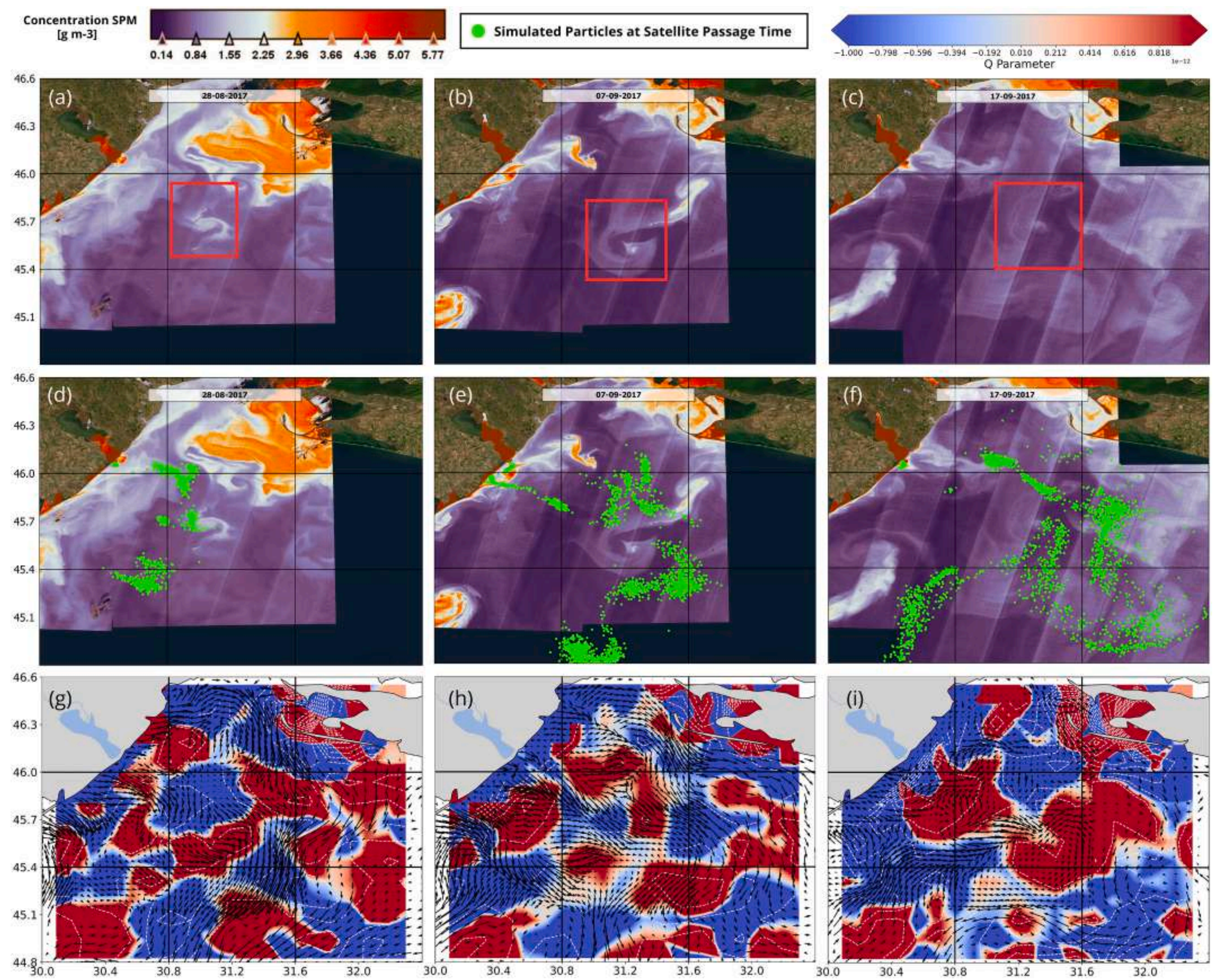

Fig. 8. Comparison of particle trajectories of the C2 simulation and observed plume dynamics in the northwestern Area. Panels (a), (b), and (c) show the SPM (Suspended Particulate Matter) plume from the Dniester River, extracted from Sentinel-2 satellite imagery on August 28th, September 7th, and September 17th, respectively, highlighting the formation and expansion of vortices (red boxes). (d), (e), and (f) overlay simulated particles (shown in green). (g), (h), and (i) overlay *Q* parameter contours onto the mean daily velocity field used in the model. Basemap sources: Esri, "World Imagery", DigitalGlobe, GeoEye, i-cubed, USDA FSA, USGS, AEX, Getmapping, Aerogrid, IGN, IGP, swisstopo, and the GIS User Community. (For interpretation of the references to colour in this figure legend, the reader is referred to the web version of this article.)

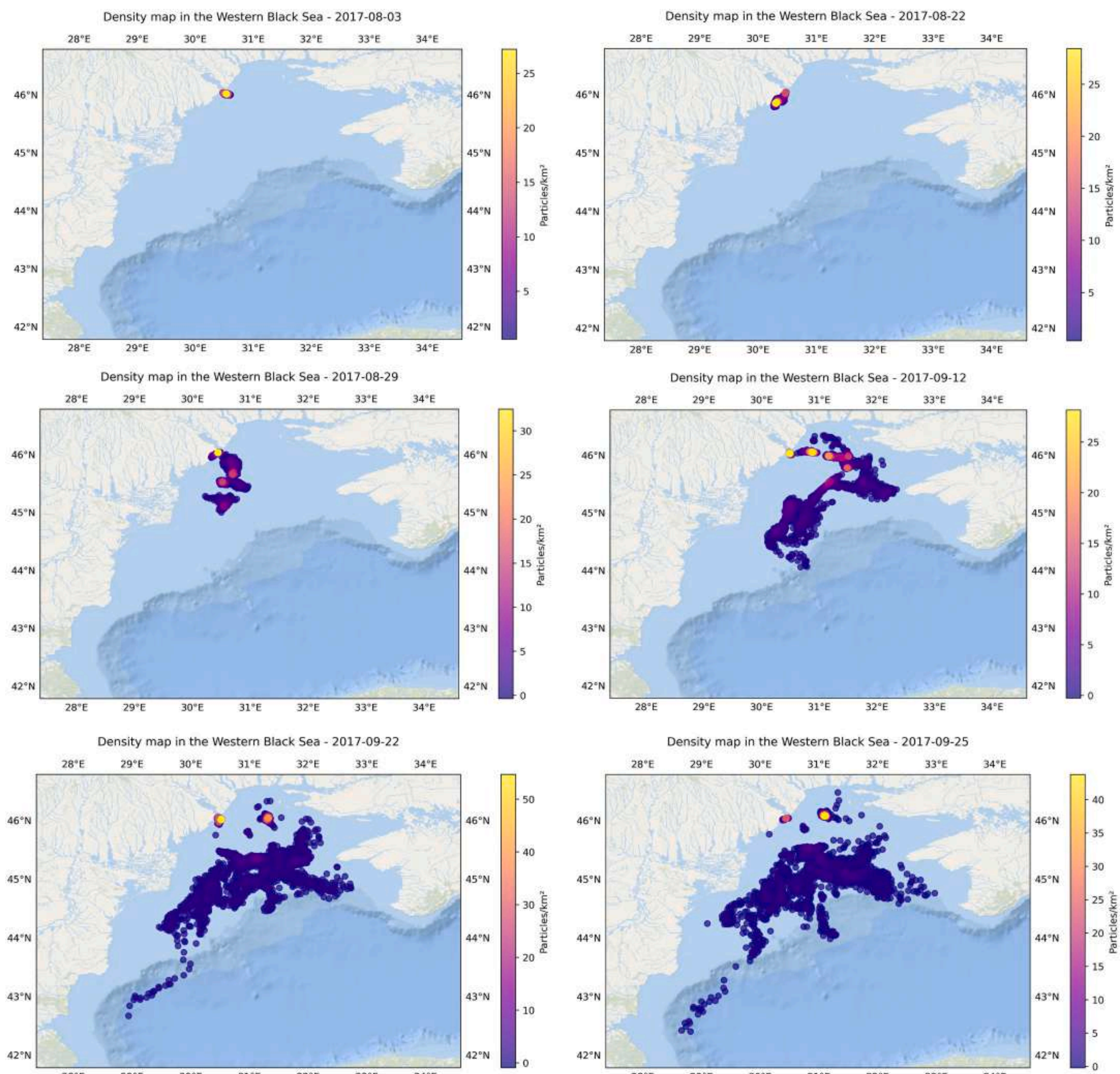

Fig. 9. Spatial distribution of particle accumulation zones in the northwest area of the simulation domain on various dates: (a) August 3rd, (b) August 22nd, (c) August 29th, (d) September 12th, (e) September 22nd, and (f) September 25th. The images depict particle density (particles/km^2), illustrating the evolving patterns of high particle concentration over time. Basemap sources: Esri, "Ocean Basemap", GEBCO, NOAA, National Geographic, DeLorme, HERE, Geonames.org, and other contributors.

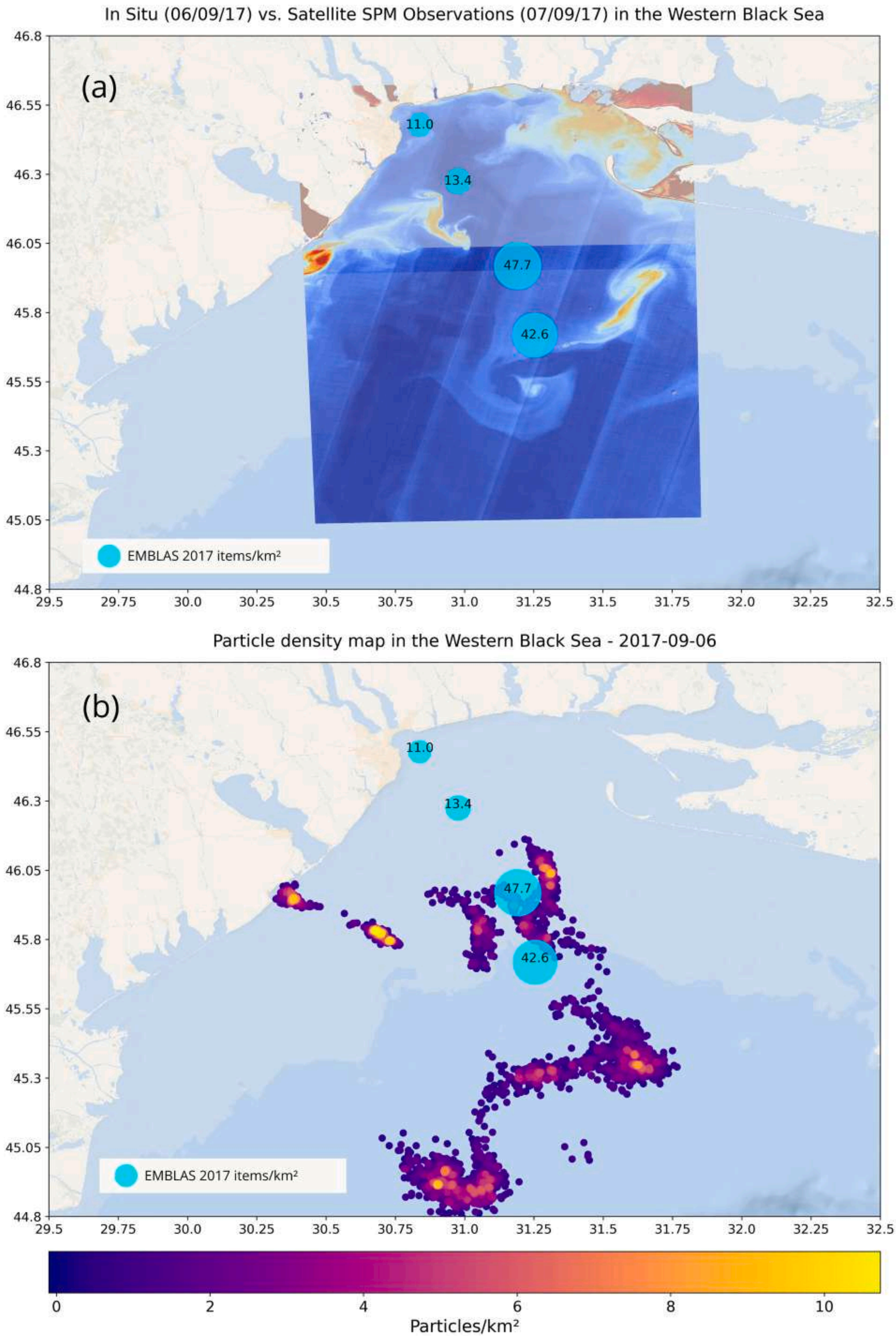

(caption on next page)

Fig. 10. Comparison of simulated particle density distribution with observed Floating Marine Macro Litter (FMML) concentrations during the 2017 EMBLAS campaign by González-Fernández et al. (2022). Panel (a) shows the satellite-derived Suspended Particulate Matter (SPM) image obtained a day before counting. Panel (b) presents our density analysis of particles on the same counting day, revealing areas of high concentration near the counting points. Basemap sources: Esri, "Ocean Basemap", GEBCO, NOAA, National Geographic, DeLorme, HERE, Geonames.org, and other contributors.

In this sense, future work should aim to incorporate additional particle attributes, such as buoyancy, density, or its ability to be resuspended, to simulate the distinct behaviors of microplastics and macroplastics more accurately. This refinement will enable a more comprehensive understanding of marine litter dynamics, including vertical transport processes and accumulation patterns in different environmental compartments, such as the water column, seabed, and coastline.

3.5. Exploring the role of SPM in understanding riverine litter dynamics in the Dniester: a preliminary discussion

While the correlation analysis between SPM and riverborne litter (macro or micro) remains in a preliminary phase due to the lack of in situ measurements necessary for local validation of remote sensing SPM algorithms, this qualitative analysis provides a basic overview of the fate of materials discharged into the Dniester River. This approach is justified by the recognition of rivers as significant conduits for plastic entering the ocean, contributing substantially to FML (Lebreton et al., 2019; Slobodnik et al., 2022; Pojar et al., 2021). As part of this process, SPM encompasses all particles larger than 0.7 μm, including microplastics (MP). These MPs, which form a considerable portion of suspended particles, can either remain on the surface or sink due to agglomeration (Sullivan et al., 2023; Rochman et al., 2019), linking them closely to riverborne litter transport.

On the other hand, MP, whether formed from the breakdown of larger plastics through weathering and fragmentation or introduced directly, can become part of the marine environment, eventually sinking and accumulating on the seabed and providing a historical record of litter deposition (Thompson et al., 2004; Kvale et al., 2020; Andrady, 2011). This process is evident in the Dniester River, as measurements by Cincinelli et al. (2021) show high microplastic accumulation near the Dniester river mouth and Odesa. These microplastics can be present within the SPM before settling. The accumulation near the Dniester likely results from particle trapping caused by regional vorticity and circulation patterns, while the Odesa area's accumulation may stem from other pollution sources, such as waste from local activities and influence from the Dnieper-Bug, contributing to hotspots on the Northwestern Shelf.

Understanding these dynamics can serve as a tool for decision-making to reduce pollution in this area and protect nearby natural zones, such as the Tuzlovski Lagoons National Park, and the overall biodiversity of the Ukrainian coast.

4. Conclusions

Although the difference in final beaching percentages between two beaching configurations C1 and C2 is minimal, spatial distribution emerges as the decisive factor. The choice between configurations hinges on factors such as computation time, which is shorter with C1 (based solely on velocities) compared to C2, which incorporates pre-calculated shoreline distances into the data used in the simulation. Additionally, the selection is contingent upon the availability and precision of shoreline data. While C1 suffices at the regional scale, C2 offers enhanced realism for coastal-scale simulations where varying resolutions are applied.

The contribution of the Dniester River to pollution in the northwestern Black Sea is evident, influenced by circulation patterns and the anticyclonic activity of the Sevastopol Eddy. This influence is noticeable in both coastal accumulation, which is notably concentrated around the mouth of the Dniester River in the Zatoka region, and in open waters within the Northwestern Shelf (NWS), revealing complex coastal transport dynamics.

Comparisons with previous regional models and in situ measurements of microplastics (MP) in sediments, along with satellite-derived Suspended Particulate Matter (SPM) observations and data from the 2017 EMBLAS campaign, validate both the model's capability to simulate Floating Marine Litter (FML) dispersion and the utility of nested grids for coastal simulation. This approach allows the reproduction of mesoscale phenomena, showing patterns consistent with observations in areas of Floating Marine Macro Litter (FMML) accumulation in both coastal and open waters.

The study indicates a potential correlation between satellite SPM observations and MP in the Dniester River and the northwestern Black Sea. High-resolution satellite-derived SPM maps show promise for estimating MP concentrations, suggesting avenues for future research to explore this relationship in greater detail.

Gaining insight into FML accumulation patterns is crucial for effective coastal management and environmental conservation. Integrated monitoring strategies and policy interventions are essential to mitigate the impact of FML on coastal ecosystems and human health in the northwestern Black Sea region.

Future research aims to integrate high-resolution hydrodynamic data across the entire western Black Sea into FML modeling efforts, enhancing understanding of its complex dynamics.

CRediT authorship contribution statement

Leidy M. Castro-Rosero: Writing – review & editing, Writing – original draft, Software, Methodology, Investigation, Formal analysis, Data curation, Conceptualization. **Ivan Hernandez:** Writing – review & editing, Software, Methodology, Data curation, Conceptualization. **Marc Mestres:** Writing – review & editing, Software, Resources, Methodology, Data curation. **Maria Liste:** Writing – review & editing, Supervision, Data curation, Conceptualization. **Jose M. Alsina:** Writing – review & editing, Supervision, Software, Resources, Project administration, Investigation, Funding acquisition, Conceptualization. **Manuel Espino:** Writing – review & editing, Supervision, Resources, Project administration, Investigation, Funding acquisition, Conceptualization.

Declaration of competing interest

The authors declare that they have no known competing financial interests or personal relationships that could have appeared to influence the work reported in this paper.

Appendix A. Satellite processed images

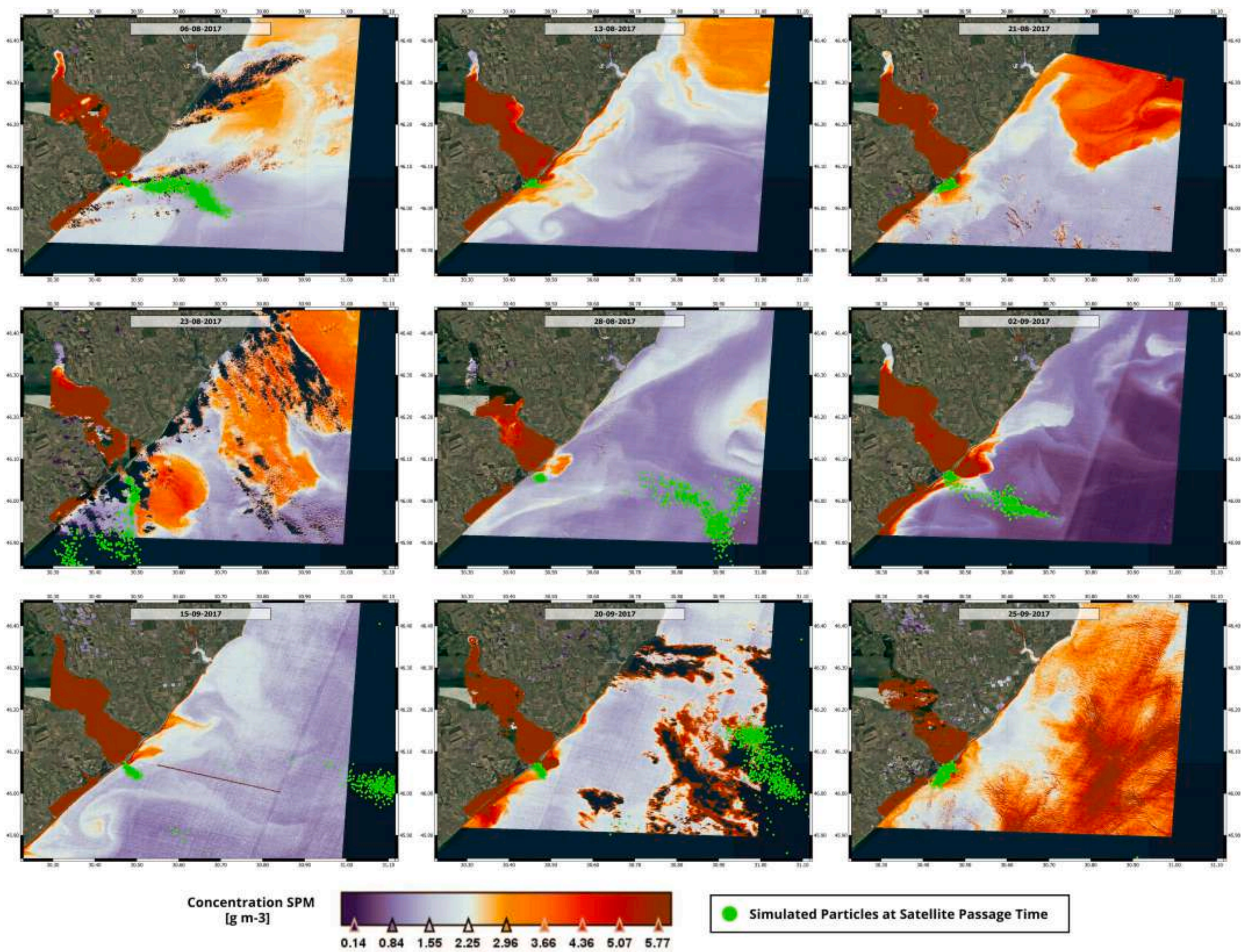

Fig. A.11. Remaining images. Comparison between the results of the C2 (green particles) simulation and the SPM (Suspended Particulate Matter) plume from the mouth of the Dniester River, extracted from Sentinel-2 satellite imagery. Basemap sources: Esri, "World Imagery", DigitalGlobe, GeoEye, i-cubed, USDA FSA, USGS, AEX, Getmapping, Aerogrid, IGN, IGP, swisstopo, and the GIS User Community.

Data availability

Data will be made available on request.

References

Alsina, J.M., Jongedijk, C.E., van Sebille, E., 2020. Laboratory measurements of the wave-induced motion of plastic particles: influence of wave period, plastic size and plastic density. J. Geophys. Res. Oceans 125, e2020JC016294. https://doi.org/10.1029/2020JC016294.

Andrady, A.L., 2011. Microplastics in the marine environment. Mar. Pollut. Bull. 62, 1596–1605. https://doi.org/10.1016/j.marpolbul.2011.05.030.

Atwood, E.C., Falcieri, F.M., Piehl, S., Bochow, M., Matthies, M., Franke, J., Carniel, S., Sclavo, M., Laforsch, C., Siegert, F., 2019. Coastal accumulation of microplastic particles emitted from the Po River, Northern Italy: comparing remote sensing and hydrodynamic modelling with in situ sample collections. Mar. Pollut. Bull. 138, 561–574. https://doi.org/10.1016/j.marpolbul.2018.11.045.

Brockmann, C., Doerffer, R., Peters, M., Kerstin, S., Embacher, S., Ruescas, A., 2016. Evolution of the C2RCC neural network for sentinel 2 and 3 for the retrieval of ocean colour products in normal and extreme optically complex waters. In: Proceedings of the Living Planet Symposium, L. Ouwehand, Czech Republic, p. 54.

Castro-Rosero, L.M., Hernandez, I., Alsina, J.M., Espino, M., 2023. Transport and accumulation of floating marine litter in the Black Sea: insights from numerical modeling. Front. Mar. Sci. 10. https://doi.org/10.3389/fmars.2023.1213333.

Cincinelli, A., Scopetani, C., Chelazzi, D., Martellini, T., Pogojeva, M., Slobodnik, J., 2021. Microplastics in the Black Sea sediments. Sci. Total Environ. 760, 143898. https://doi.org/10.1016/j.scitotenv.2020.143898.

D'Asaro, E.A., Shcherbina, A.Y., Klymak, J.M., Molemaker, J., Novelli, G., Guigand, C. M., Haza, A.C., Haus, B.K., Ryan, E.H., Jacobs, G.A., Huntley, H.S., Laxague, N.J.M., Chen, S., Judt, F., McWilliams, J.C., Barkan, R., Kirwan, A.D., Poje, A.C., Özgökmen, T.M., 2018. Ocean convergence and the dispersion of flotsam. Proc. Natl. Acad. Sci. 115, 1162–1167. https://doi.org/10.1073/pnas.1718453115.

Delandmeter, P., van Sebille, E., 2019. The parcels v2.0 Lagrangian framework: new field interpolation schemes. Geosci. Model Dev. 12, 3571–3584. https://doi.org/10.5194/gmd-12-3571-2019. publisher: Copernicus GmbH.

Forsberg, P.L., Sous, D., Stocchino, A., Chemin, R., 2020. Behaviour of plastic litter in nearshore waters: first insights from wind and wave laboratory experiments. Mar. Pollut. Bull. 153, 111023. https://doi.org/10.1016/j.marpolbul.2020.111023.

Ginzburg, A.I., Kostianoy, A.G., Nezlin, N.P., Soloviev, D.M., Stanichny, S.V., 2002. Anticyclonic eddies in the northwestern Black Sea. J. Mar. Syst. 32, 91–106. https://doi.org/10.1016/S0924-7963(02)00035-0.

González-Fernández, D., Hanke, G., Pogojeva, M., Machitadze, N., Kotelnikova, Y., Tretiak, I., Savenko, O., Bilashvili, K., Gelashvili, N., Fedorov, A., Kulagin, D., Terentiev, A., Slobodnik, J., 2022. Floating marine macro litter in the Black Sea: toward baselines for large scale assessment. Environ. Pollut. 309, 119816. https://doi.org/10.1016/j.envpol.2022.119816.

Harris, P.T., Westerveld, L., Nyberg, B., Maes, T., Macmillan-Lawler, M., Appelquist, L.R., 2021. Exposure of coastal environments to river-sourced plastic pollution. Sci. Total Environ. 769, 145222. https://doi.org/10.1016/j.scitotenv.2021.145222.

Hernandez, I., Castro-Rosero, L.M., Espino, M., Alsina Torrent, J.M., 2024. LOCATE v1.0: numerical modelling of floating marine debris dispersion in coastal regions using parcels v2.4.2. Geosci. Model Dev. 17, 2221–2245. https://doi.org/10.5194/gmd-17-2221-2024.

Iemelianov, V.O., Nasiedkin, Y.I., Kukovska, T.S., Mytrofanova, O.A., Dovbysh, S.M., 2024. Research of plastics and microplastics in the Black Sea geoecosystem as a component of its pollution assessment. Ukrainian geographical journal 2023, 26–35. https://doi.org/10.15407/ugz2023.04.026.

Isern-Fontanet, J., García-Ladona, E., Font, J., 2003. Identification of marine eddies from altimetric maps. J. Atmos. Ocean. Technol. 20, 772–778. https://doi.org/10.1175/1520-0426(2003)20<772:IOMEFA>2.0.CO;2.

Karageorgis, A.P., Kourafalou, V.H., Anagnostou, C., Tsiaras, K.P., Raitsos, D.E., Papadopoulos, V., Papadopoulos, A., 2009. River-induced particle distribution in the northwestern Black Sea (September 2002 and 2004). J. Geophys. Res. Oceans 114. https://doi.org/10.1029/2009JC005460.

Kubryakov, A.A., Stanichny, S.V., 2015. Seasonal and interannual variability of the Black Sea eddies and its dependence on characteristics of the large-scale circulation. Deep-Sea Res. I Oceanogr. Res. Pap. 97, 80–91. https://doi.org/10.1016/j.dsr.2014.12.002.

Kubryakov, A.A., Mizyuk, A.I., Stanichny, S.V., 2024. Stationarity and separation of the Sevastopol eddies in the Black Sea: the role of eddy-topographic interaction and submesoscale dynamics. J. Mar. Syst. 241, 103911. https://doi.org/10.1016/j.jmarsys.2023.103911.

Kvale, K., Prowe, A.E.F., Chien, C.T., Landolfi, A., Oschlies, A., 2020. The global biological microplastic particle sink. Sci. Rep. 10, 16670. https://doi.org/10.1038/s41598-020-72898-4.

Kyryliuk, D., Kratzer, S., 2019. Evaluation of sentinel-3A OLCI products derived using the Case-2 regional CoastColour processor over the Baltic Sea. Sensors (Basel, Switzerland) 19, 3609. https://doi.org/10.3390/s19163609.

Lazăr, L., 2021. Impact of the Rivers on the Black Sea Ecosystem. Technical Report. ANEMONE Deliverable 2.1. Ed. CD PRESS, 225 pp. ISBN 978-606-528-528-6.

Lebedynets, M., Sprynskyy, M., Kowalkowski, T., Buszewski, B., 2005. Evaluation of hydrosphere state of the Dniester river catchment. Pol. J. Environ. Stud. 14, 65.

Lebreton, L., Egger, M., Slat, B., 2019. A global mass budget for positively buoyant macroplastic debris in the ocean. Sci. Rep. 9, 12922. https://doi.org/10.1038/s41598-019-49413-5.

Lechner, A., Keckeis, H., Lumesberger-Loisl, F., Zens, B., Krusch, R., Tritthart, M., Glas, M., Schludermann, E., 2014. The Danube so colourful: a potpourri of plastic litter outnumbers fish larvae in Europe's second largest river. Environ. Pollut. 188, 177–181. https://doi.org/10.1016/j.envpol.2014.02.006.

Martínez-Vicente, V., Clark, J.R., Corradi, P., Aliani, S., Arias, M., Bochow, M., Bonnery, G., Cole, M., Cózar, A., Donnelly, R., Echevarría, F., Galgani, F., Garaba, S.P., Goddijn-Murphy, L., Lebreton, L., Leslie, H.A., Lindeque, P.K., Maximenko, N., Martin-Lauzer, F.R., Moller, D., Murphy, P., Palombi, L., Raimondi, V., Reisser, J., Romero, L., Simis, S.G.H., Sterckx, S., Thompson, R.C., Topouzelis, K.N., van Sebille, E., Veiga, J.M., Vethaak, A.D., 2019. Measuring marine plastic debris from space: initial assessment of observation requirements. Remote Sens. 11, 2443. https://doi.org/10.3390/rs11202443.

Miladinova, S., Macias, D., Stips, A., Garcia-Gorriz, E., 2020. Identifying distribution and accumulation patterns of floating marine debris in the Black Sea. Mar. Pollut. Bull. 153, 110964. https://doi.org/10.1016/j.marpolbul.2020.110964.

Oguz, T., Aubrey, D., Latun, V., Demirov, E., Koveshnikov, L., Sur, H., Diaconu, V., Besiktepe, S., Duman, M., Limeburner, R., Eremeev, V., 1994. Mesoscale circulation and thermohaline structure of the Black Sea observed during HydroBlack '91. Deep-Sea Res. I Oceanogr. Res. Pap. 41, 603–628. https://doi.org/10.1016/0967-0637(94)90045-0.

Okubo, A., 1970. Horizontal dispersion of floatable particles in the vicinity of velocity singularities such as convergences. Deep-Sea Res. Oceanogr. Abstr. 17, 445–454. https://doi.org/10.1016/0011-7471(70)90059-8.

Piehl, S., Atwood, E.C., Bochow, M., Imhof, H.K., Franke, J., Siegert, F., Laforsch, C., 2020. Can water constituents be used as proxy to map microplastic dispersal within transitional and coastal waters? Front. Environ. Sci. 8, 92. https://doi.org/10.3389/fenvs.2020.00092.

Pojar, I., Kochleus, C., Dierkes, G., Ehlers, S.M., Reifferscheid, G., Stock, F., 2021. Quantitative and qualitative evaluation of plastic particles in surface waters of the Western Black Sea. Environ. Pollut. 268, 115724. https://doi.org/10.1016/j.envpol.2020.115724.

Rochman, C.M., Brookson, C., Bikker, J., Djuric, N., Earn, A., Bucci, K., Athey, S., Huntington, A., McIlwraith, H., Munno, K., De Frond, H., Kolomijeca, A., Erdle, L., Grbic, J., Bayoumi, M., Borrelle, S.B., Wu, T., Santoro, S., Werbowski, L.M., Zhu, X., Giles, R.K., Hamilton, B.M., Thaysen, C., Kaura, A., Klasios, N., Ead, L., Kim, J., Sherlock, C., Ho, A., Hung, C., 2019. Rethinking microplastics as a diverse contaminant suite. Environ. Toxicol. Chem. 38, 703–711. https://doi.org/10.1002/etc.4371.

Sadighrad, E., Fach, B.A., Arkin, S.S., Salihoğlu, B., Hüsrevoğlu, Y.S., 2021. Mesoscale eddies in the Black Sea: characteristics and kinematic properties in a high-resolution ocean model. J. Mar. Syst. 223, 103613. https://doi.org/10.1016/j.jmarsys.2021.103613.

Safranov, T.A., Berlinsky, N.A., Zmienko, D.M., 2020. Plastic of the solid domestic waste on the coastal zone of the northwestern part of the Black Sea as a component of marine litter. Visnyk of V. N. Karazin Kharkiv National University series Ecology 57–66. https://doi.org/10.26565/1992-4259-2020-23-06.

van Sebille, E., Aliani, S., Law, K.L., Maximenko, N., Alsina, J.M., Bagaev, A., Bergmann, M., Chapron, B., Chubarenko, I., Cózar, A., Delandmeter, P., Egger, M., Fox-Kemper, B., Garaba, S.P., Goddijn-Murphy, L., Hardesty, B.D., Hoffman, M.J., Isobe, A., Jongedijk, C.E., Kaandorp, M.L., Khatmullina, L., Koelmans, A.A., Kukulka, T., Laufkötter, C., Lebreton, L., Lobelle, D., Maes, C., Martinez-Vicente, V., Morales Maqueda, M.A., Poulain-Zarcos, M., Rodríguez, E., Ryan, P.G., Shanks, A.L., Shim, W.J., Suaria, G., Thiel, M., Van Den Bremer, T.S., Wichmann, D., 2020. The physical oceanography of the transport of floating marine debris. Environ. Res. Lett. 15, 23003. https://doi.org/10.1088/1748-9326/ab6d7d. publisher: IOP Publishing.

Shekk, P., 2015. Ichthyofauna of water bodies of the National Nature Park "Tuzla lagoons" and its commercial fisheries exploitation. Fisheries Science of Ukraine 5–19. https://doi.org/10.15407/fsu2015.02.005.

Slobodnik, J., Arabidze, M., Mgeladze, M., Korshenko, A., Mikaelyan, A., Komorin, V., Minicheva, G., 2022. EMBLAS Final Scientific Report. Technical Report. Serednіak T. K, Dnipro. ISBN: 978-617-8111-01-4.

Stanev, E.V., Ricker, M., 2019. The fate of marine litter in semi-enclosed seas: a case study of the Black Sea. Front. Mar. Sci. 6, 1–16. https://doi.org/10.3389/fmars.2019.00660.

Strokal, V., Kuiper, E.J., Bak, M.P., Vriend, P., Wang, M., Van Wijnen, J., Strokal, M., 2022. Future microplastics in the Black Sea: river exports and reduction options for zero pollution. Mar. Pollut. Bull. 178, 113633. https://doi.org/10.1016/j.marpolbul.2022.113633.

Suaria, G., Melinte-Dobrinescu, M.C., Ion, G., Aliani, S., 2015. First observations on the abundance and composition of floating debris in the North-western Black Sea. Mar. Environ. Res. 107, 45–49. https://doi.org/10.1016/j.marenvres.2015.03.011.

Sullivan, E., Cole, M., Atwood, E.C., Lindeque, P.K., Chin, P.T., Martinez-Vicente, V., 2023. In situ correlation between microplastic and suspended particulate matter concentrations in river-estuary systems support proxies for satellite-derived estimates of microplastic flux. Mar. Pollut. Bull. 196, 115529. https://doi.org/10.1016/j.marpolbul.2023.115529.

Thompson, R.C., Olsen, Y., Mitchell, R.P., Davis, A., Rowland, S.J., John, A.W.G., McGonigle, D., Russell, A.E., 2004. Lost at sea: where is all the plastic? Science 304, 838. https://doi.org/10.1126/science.1094559.

Veettil, B.K., Hong Quan, N., Hauser, L.T., Doan Van, D., Quang, N.X., 2022. Coastal and marine plastic litter monitoring using remote sensing: a review. Estuar. Coast. Shelf Sci. 279, 108160. https://doi.org/10.1016/j.ecss.2022.108160.

Vespremeanu, E., Golumbeanu, M., 2018. Catchment area of the black sea. In: Vespremeanu, E., Golumbeanu, M. (Eds.), The Black Sea. Springer International Publishing, pp. 15–25. https://doi.org/10.1007/978-3-319-70855-3_3.

Waqas, M., Wong, M., Stocchino, A., Abbas, S., Hafeez, S., Zhu, R., 2023. Marine plastic pollution. Mar. Pollut. Bull. https://doi.org/10.1016/j.marpolbul.2023.115746.

Weiss, J., 1991. The dynamics of enstrophy transfer in two-dimensional hydrodynamics. Physica D: Nonlinear Phenomena 48, 273–294. https://doi.org/10.1016/0167-2789(91)90088-Q.

Zhou, F., Shapiro, G., Wobus, F., 2014. Cross-shelf exchange in the northwestern Black Sea. J. Geophys. Res. Oceans 119, 2143–2164. https://doi.org/10.1002/2013JC009484.